Mechanics of Materials 41 (2009) 1000–1016

Contents lists available at ScienceDirect

Mechanics of Materials

journal homepage: www.elsevier.com/locate/mechmat

Probabilistic inverse problem and system uncertainties for damage detection in piezoelectrics

Roberto Palma *, Guillermo Rus, Rafael Gallego

Structural Mechanics & Hydraulic Engineering, University of Granada, 18071 Granada, Spain

ARTICLE INFO

Article history:
Received 1 July 2008
Received in revised form 9 February 2009

ABSTRACT

This paper provides a probabilistic formulation to design a monitoring setup for damage detection in piezoelectric plates, solving a model-based identification inverse problem (IP). The IP algorithm consists on the minimization of a cost functional defined as the quadratic-difference between experimental and trial measurements simulated by the finite element method. The motivation of this work comes from the necessity for a more rational design criteria applied to damage monitoring of piezoelectric materials. In addition, it is very important for the solving of the inverse problem to take into account the random nature of the system to be solved in order to obtain accurate and reliable solutions. In this direction, two investigations are considered. For the first, the experimental measurements are simulated combining a finite element and a Monte Carlo analysis, both validated with already published results. Then, an uncertainty analysis is used to obtain the statistical distribution of the simulated experimental measurements, while a sensitivity analysis is employed to find out the influence of the uncertainties in the model parameters related to the measurement noise. Upon the study of the measurements, they are used as the input for the damage identification IP which produces the location and extension of a defect inside a piezoelectric plate. For the second investigation, a probabilistic IP approach is developed to determine the statistical distribution and sensitivities of the IP solutions. This novel approach combines the Monte Carlo and the IP algorithm, considering the trial measurements as random. In conclusion, the analysis demonstrates that in order to improve the quality of the damage characterization, only a few material parameters have to be controlled at the experimental stage. It is important to note that this is not an experimental study, however, it can be considered as a first step to design a rational damage identification experimental device, controlling the variables that increase the noise level and decrease the accuracy of the IP solution.

1. Introduction

Piezoelectric ceramics are widely used in electromechanical devices due to their coupling between the electric and mechanical energies. They are used as sensors and actuators in Structural Health Monitoring, Intelligent Structures, etc. However, these ceramics are brittle and susceptible to fracture, shortcoming that limits their performance. In the last decades, many analytical, numerical and experimental works about fracture mechanics have emerged in the literature. Nevertheless, there are few studies about damage detection, despite it is an interesting way to prevent the failure of these ceramics.

In recent years, identification inverse problems have been developed in a variety of continuum mechanics applications (see Liu and Chen, 1996; Rus et al., 2006; Tardieu and Constantinescu, 2000; Bonnet and Constantinescu, 2005; Tarantola, 2005). Specifically, for the piezoelectric ceramics, inverse problem techniques have been applied to determine their elastic, dielectric and coupling properties.

* Corresponding author. Tel.: +34 958249515; fax: +34 958242719.
E-mail addresses: rpalgue@ugr.es (R. Palma), grus@ugr.es (G. Rus), gallego@ugr.es (R. Gallego).

0167-6636/$ - see front matter © 2009 Elsevier Ltd. All rights reserved.
doi:10.1016/j.mechmat.2009.05.001

For example, Kaltenbacher et al. (2006) defined a cost functional as the difference between electric impedances observed in laboratory and those obtained after solving the direct problem by the finite element method (FEM). A similar cost functional was used in Ruíz et al. (2004a,b), which was minimized using genetic algorithms. On the other hand, Araújo et al. (2002, 2006) proposed an inverse problem to obtain the constitutive properties of composite plate specimens with surface bonded piezoelectric patches or layers, where the cost functional was the difference between the experimental and FEM-predicted eigen-frequencies and its minimization was carried out using two strategies: a gradient-based method, and neural networks. Finally, in Rus et al. (2009) an identification inverse problems was applied to find defects in piezoelectric plates, obtaining the optimal experimental configuration based on probability of detection studies.

Rus et al. (2009) concluded that the inverse problem solution strongly depends of the noise level on the experimental measurement. If the systematic errors are neglected, this noise level is related to the inherent randomness of the material properties and excitation loads. Note that Oden et al. (2003) reported the treatment of physical uncertainties is a research area of great importance for the structural mechanics community. According to this treatment, several questions emerge: what is the sensitivity of the inverse problem solution to system uncertainties?, which are the main variables responsible for the experimental noise? and how can it be effectively reduced?

To answer these questions, an inverse problem to find a defect in a piezoelectric plates is formulated in this work. The cost functional is defined as the quadratic-difference between experimental and simulated measurements. The simulated measurements are obtained by solving the direct problem using a FEM with optimized meshes, whereas the experimental measurements are also simulated in order to carry out a controlled uncertainty and sensitivity analysis. The latter simulation is performed using two procedures: (i) adding a noise normality distributed to the FEM-simulated measurement and (ii) using Monte Carlo techniques, together with the FEM, and considering the material properties as normally distributed variables. Subsequently, the two procedures, (i) and (ii), are compared and, for the case (ii), a sensitivity analysis is performed in order to determine which variables are responsible of increasing the experimental noise level. Finally, a probabilistic inverse problem approach is performed, combining the Monte Carlo analysis and the inverse problem solution (obtained minimizing the cost functional by genetic algorithms). This approach is applied for the two procedures (i) and (ii), obtaining the sensitivities of the inverse problem solutions to system uncertainties and analyzing the way to obtain accurate solutions.

These formulations are applied to solve the relationships between system model, observations (measurements) and IP solution (damage characterization parameters), in a deterministic and in a probabilistic way through the results depicted in the flow chart of Fig. 1.

In conclusion, a few properties must to be calculated with a controlled error to obtain a satisfactory result using the inverse problem technique. Although this is not an experimental study, it can be considered as a first step to design a rational damage identification experimental device, controlling the variables that increase the noise level and decrease the accuracy of the inverse problem solution.

2. Monte Carlo analysis

The Monte Carlo analysis (MCA) has been applied in many research areas, like geophysics (see, Tarantola, 2005) or structural mechanics (see, Charmpis and Scheller,

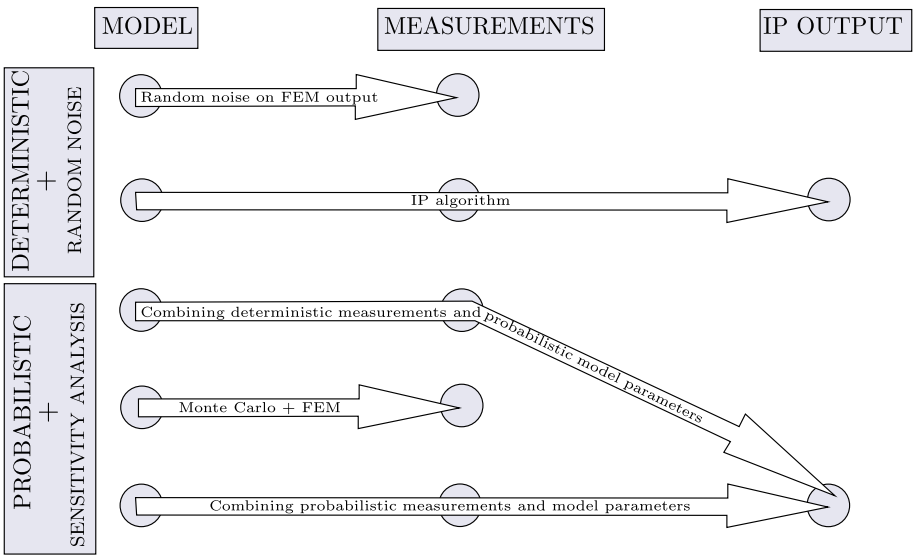

Fig. 1. Flow chart of the results obtained to study the relationships between system model, observations (measurements) and IP solution (damage characterization parameters), in a deterministic and in a probabilistic way.

2006). The idea behind the MCA (an allusion to the famous Casino) is old, but its application to the solution of scientific problems is closely connected to the advent of modern computers.

Consider a physical model represented by:

$$\phi_i = M(\xi_j) \tag{1}$$

where ϕ_i are the i dependent or observable variables, ξ_j are the j independent variables, model parameters or random variables (this last denomination is the form used in the following) and M describes the model. MCA consists in performing multiple evaluations of a sample of the random variables. In general, MCA involves the five steps, see Saltelli et al. (2000), shown in Fig. 2:

1. *Selection of distribution functions for the random variables* ξ_j. Distribution functions are chosen depending of the type of problem (see Clemen and Winkler (1999) for a revision of the models, their selection and their calibration).
2. *Generation of the sample*. Many sampling procedures can be used. However, two types are the most important: (i) a random sampling is easy to implement and provides unbiased estimates for means, variances and distribution functions (this procedure is preferred when sufficiently large samples can be evaluated) and (ii) a Latin hypercube sampling (see Cochran, 1977) is used when large samples are not computationally practicable.
3. *Evaluation of the model*. The model M is executed using numerical or analytical techniques. These can be seen by the MCA as a *black box*.
4. *Uncertainty analysis* (UA). The purpose of UA is to determinate the uncertainty in estimates for the observable variables ϕ_i when the uncertainties in random variables ξ_j are known. Thus, the probability distribution function (PDF) and cumulative distributions function (CDF) are obtained. They allow an easy extraction of the probabilities of having values in different subsets of the range of ϕ_i. Furthermore, two scalar variables, the mean μ and the standard deviation σ, can summarize the uncertainty in scalar-valued results. These scalar variables are calculated by (see Saltelli et al., 2000):

$$\mu = \frac{1}{m}\sum_{i=1}^{m}\phi_i; \quad \text{Variance} = \frac{1}{m-1}\sum_{i=1}^{m}(\phi_i - \mu)^2 \tag{2}$$

where m is the number of executions of the model or sample size.

5. *Sensitivity analysis* (SA). The goal of SA is to determine the relationships between the uncertainty in the random variables ξ_j used in the analysis and the uncertainty in the observable variables ϕ_i. This is a method for checking the quality of a given model. There are many available procedures to develop the SA, however we use multiple linear regression, see Montgomery and Runger (1999), which provides a relationship between ξ_j and ϕ approximating M by means of:

$$\phi \approx \sum_{j=1}^{N_\xi}\theta_j\xi_j + \Psi \tag{3}$$

where, N_ξ is the number of random variables, θ_j are the regression coefficients, that can be used to indicate the importance of individual random variables ξ_j with respect to the uncertainty in the output ϕ, and Ψ is the error of the approximation. The multiple linear regression is aimed at finding the θ_j parameters that minimize Ψ. For this purpose, at least N_ξ observations or simulations ϕ are required. The degree to which random variables are related to the dependent variable is expressed by the correlation coefficient (R). Thus, the closer R^2 is to unity, the better is the model performance.

Standardized regression coefficients are defined in Mayer and Younger (1974) by:

$$\Theta_j = \theta_j\frac{\sigma_{\xi_j}}{\sigma_\phi} \tag{4}$$

and, when the ξ_j are independent, its absolute value can be used to provide a measure of variable importance. Calculating Θ_j is equivalent to performing the regression analysis with the input and output variables normalized to mean zero and standard deviation one.

3. Problem description

The non-destructive evaluation (NDE) technique for damage detection consists of a system where the tested sample is excited and its response is measured, in order to infer or reconstruct the damage status that is responsible for the alteration of the measurement in comparison with the non-damaged state. Therefore, the first step to

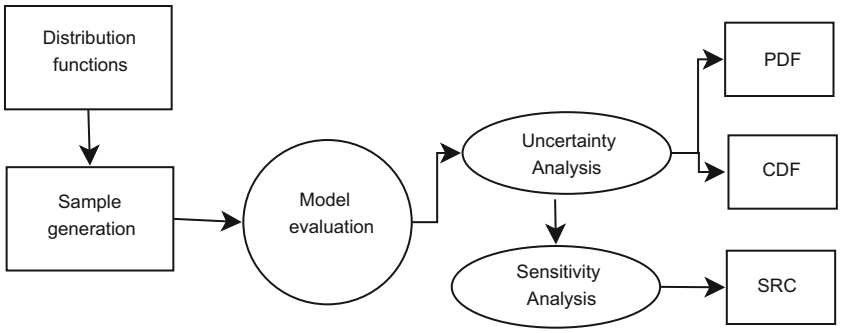

Fig. 2. Flow chart to compute the probability distribution function (PDF), cumulative distribution function (CDF) and standardized regression coefficients (SRC) using the Monte Carlo analysis.

apply a NDE technique is the election of the system, comprised by the specimen and the excitation and measurement techniques.

3.1. Specimen

The NDE configuration considered for damage detection in this work is shown in Fig. 3. The system consists in a 3-D piezoelectric solid of dimensions ($L_x \times L_y \times L_z$), where the damage to be found is a circular defect of radius r and centered at (x_0, z_0).

The material is a piezoelectric ceramic, which has the ability to generate an electric charge in response to applied mechanical stress and vice versa. From a mathematical point of view, the piezoelectric constitutive equations in the form strain–voltage are given by EFUNDA – Engineering Fundamentals (2006) as:

$$\mathbf{S} = \mathbf{s}^D\mathbf{T} + \mathbf{g}^t\mathbf{D}; \quad \mathbf{E} = -\mathbf{g}\mathbf{T} + \boldsymbol{\beta}^T\mathbf{D} \tag{5}$$

where **S**, **T**, **E** and **D** denote deformation, stress, electric field and electric displacement or induction. On the other hand, $\mathbf{s}^D$, **g** and $\boldsymbol{\beta}^T$ denote elastic properties measured to open circuit $(.)^D$, coupling and dielectric properties measures to constant stress $(.)^T$. In matrix form:

$$\mathbf{s}^D = \begin{bmatrix} s^D_{11} & s^D_{12} & s^D_{13} & 0 & 0 & 0 \\ s^D_{12} & s^D_{11} & s^D_{13} & 0 & 0 & 0 \\ s^D_{13} & s^D_{13} & s^D_{33} & 0 & 0 & 0 \\ 0 & 0 & 0 & s^D_{44} & 0 & 0 \\ 0 & 0 & 0 & 0 & s^D_{44} & 0 \\ 0 & 0 & 0 & 0 & 0 & 2(s^D_{11} - s^D_{12}) \end{bmatrix};$$

$$\mathbf{g} = \begin{bmatrix} 0 & 0 & 0 & 0 & g_{15} & 0 \\ 0 & 0 & 0 & g_{15} & 0 & 0 \\ g_{31} & g_{31} & g_{33} & 0 & 0 & 0 \end{bmatrix}; \tag{6}$$

$$\boldsymbol{\beta}^T = \begin{bmatrix} \beta^T_{11} & 0 & 0 \\ 0 & \beta^T_{11} & 0 \\ 0 & 0 & \beta^T_{33} \end{bmatrix}$$

Eq. (6) is also expressed in *reduced* or *effective* form in order to apply the plain strain consideration (see Sosa and Khutoryansky, 1996).

The plain strain consideration is assumed in this work. This assumption is appropriate to simulate a transverse section of a standard piezoelectric specimen, in which only the plane x–z is studied. This 2-D reduction is also assumed in Sosa and Khutoryansky (1996), for analytical, and Pérez-Aparicio et al. (2007), for numerical studies about piezoelectric with defects. Considering the plain strain approximation, and in absence of body forces and electric charge density, the piezoelectric behaviour is modeled by *Gauss*' law, the equation that relate the electric field and the voltage, the mechanical equilibrium equation and the compatibility equation:

$$\begin{aligned} &\nabla \cdot \mathbf{D} = 0; \quad \mathbf{E} = -\nabla\phi \\ &\nabla^s \cdot \mathbf{T} = 0; \quad \mathbf{S} = \frac{1}{2}(\nabla\mathbf{u} + \nabla\mathbf{u}^t) \end{aligned} \tag{7}$$

where $\mathbf{u} = (u, w)$ denotes the displacement in directions x and z, respectively, and ϕ is the electric potential or voltage. Finally, the standard sign criteria is used: electric field and stress values are considered positive for the same direction of polarization **P** (see Fig. 3) of the material and for tractions, respectively.

3.2. Excitation and measurement

In order to proceed with the damage detection, the system is excited by a mechanical traction T^{ap}_{xx} transverse to the poling direction, while its response (voltage ϕ) is measured at $N_i = 25$ points equally spaced along the lower boundary of the plate, see Fig. 3. According to Rus et al. (2009), who performed an optimization of the excitation-measurement system for damage detection in piezoelectric ceramics in a previous work, this configuration provides the highest identifiability. Note that a mechanical load is applied and an electrical response is measured, and therefore a coupling effect is induced and captured in the testing.

4. Inverse problem methodology

A model-based inverse problem (IP) is applied to identify the defect shows in Fig. 3. Fig. 4 provides the flow chart

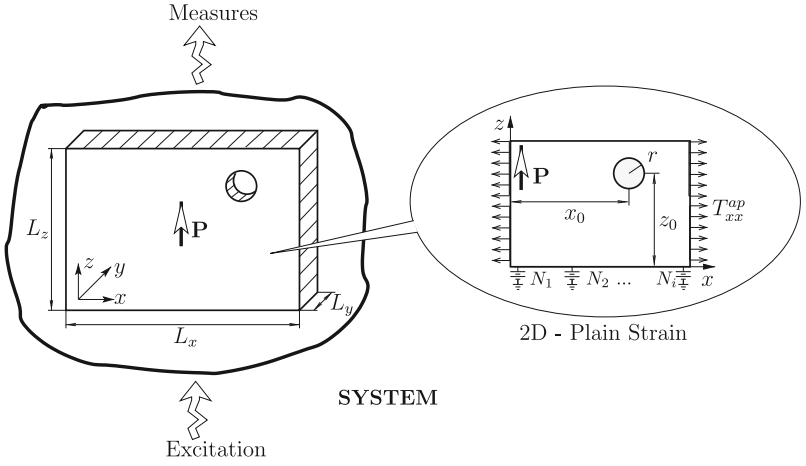

Fig. 3. Non-destructive scheme for damage detection.

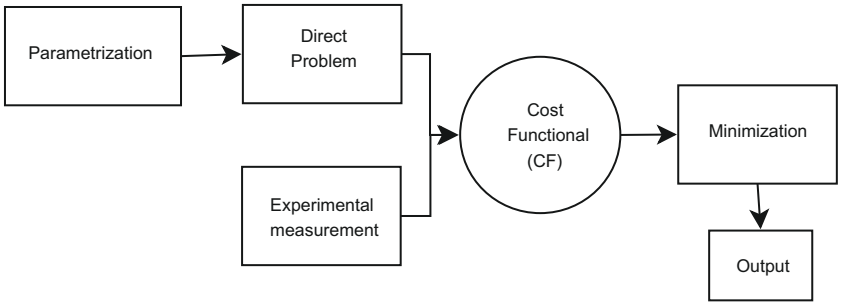

Fig. 4. Flow chart of the model-based inverse problem.

of the model-based IP, where two inputs need to be introduced: (i) the parametrization, responsible for which parameters of the model control the characterization of the sought damage and (ii) the experimental measurements. In the next step, the output of the direct problem and the experimental measurements are inserted in a cost functional (CF). Finally, the CF is minimized and the IP solution (which is given in terms of the parameters that best fit the characterization of the defect with the criteria of measurement similarity) is obtained.

4.1. Parametrization

In the context of inverse problems, parametrization of the model means to characterize the sought solution (the defect in this case) by a set of parameters, which are the working variables and the output of the IP. The choice of parametrization is not obvious, and it is a critical step in the problem setup, since the inverse problem is a badly conditioned one, in the sense that the solution may not be stable, exist or be unique, and the assumptions on the damage model that allow to represent it by a set of parameters can be understood as a strong regularization technique. In particular, a reduced set of parameters is chosen to facilitate the convergence of the search algorithm, and they are also defined to avoid coupling between them.

One should bear in mind that there is a strong relationship between the number of input and output data (number of measurements and number of output parameters), which is also responsible for the conditioning of the problem. In particular, the number of measurements must be equal or larger (preferably) than the number of parameters.

The damage location and size estimation problem presented suggests the definition of the immediate parameters x_0, z_0 to characterize the location of the center of the defect, and the radius r that represents the extent of the defect (see Fig. 3). Finally, the chosen parameters are grouped in a vector $\mathbf{p} = \{p_i\} = \{x_0, z_0, r\}$, while the true (and unknown) position and extent of the defect is represented by $\tilde{\mathbf{p}} = \{\tilde{x}_0, \tilde{z}_0, \tilde{r}\}$.

4.2. Direct problem

The direct or forward problem consists of solving the response of the piezoelectric plate shown in Fig. 3, given a specific excitation and a specific defect. In order to solve the direct problem, a numerical tool must be applied, since there are not analytical solutions for finite piezoelectric plates with a defect.

The finite element method (FEM) is the numerical method employed to solve the direct problem in this work. There are many research and commercial FEM codes that solve piezoelectric problems in the literature. However, we have used the 9-node quadratic FEM developed in Pérez-Aparicio et al. (2007) and implemented in the research academic finite element code FEAP, see Taylor et al. (2005). The commercial FEM codes can usually only be used as a *black box*, which does not allow to develop automating algorithms with sufficient flexibility, like the meshing technique used in this case, or the connection with the search algorithms in the IP.

The boundary conditions applied to the plate to solve the direct problem are shown in Fig. 5a. Note that the electric potential is set to zero along the top boundary of the plate, since it requires a reference point. On the other hand, the electric boundary condition around the defect is assumed to be of the *impermeable* type, since the defect does not need to be meshed, which improves the computational efficiency. The choice of electric boundary condition has generated controversy in recent years (see Ou and Chen (2003) for discussion). However, according to the conclusions given by Pérez-Aparicio et al. (2007) and considering the circular shape of the defect in this work, the *impermeable* electric boundary condition is a good approximation.

Fig. 5b shows the FEM mesh used, with emphasis on the cavity inside the plate representing a cavity-type defect. In this work, the fully automatic algorithm developed in Rus et al. (2009) has been used. This algorithm combines a medial axis transform, a transfinite interpolation and a stretching function of tangent hyperbolic type.

In order to determine the number of elements it is developed a convergence study, where the error on measurement point and the consumed CPU time are monitored. The error is defined by the parameter η,

$$\eta = \left| \frac{\phi^{EXA}(x_0 + r, z_0) - \phi^{FEM}(x_0 + r, z_0)}{\phi^{EXA}(x_0 + r, z_0)} \right| \times 100$$

where $\phi^{EXA}(x_0 + r, z_0)$ and $\phi^{FEM}(x_0 + r, z_0)$ are the exact and FEM-computed electric potentials at the edge of the circular cavity (where the field will show the maximum concentration, and the maximum error will be located). Since

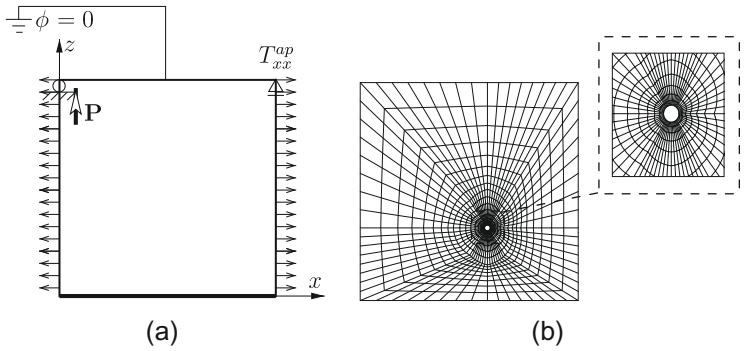

Fig. 5. (a) Boundary conditions and (b) example of the mesh used to solve the direct problem by the FEM.

there is no available analytical solution for the electric potential on the edge of a finite plate, the exact solution is estimated by a highly refined FEM mesh (using 96,000 elements).

The convergence curve is shown in Rus et al. (2009). For a mesh composed of 1176 elements the numerical error is 4.8×10^{-4}% (note that the electric field is obtained by a scalar potential with one degree of freedom by node) and the solution requires a CPU time of 6 [s] using a PC of 1 [Gb] of RAM memory and *Linux* operating system. Therefore, an optimized mesh is achieved, specially to apply to IP where, due to the optimization procedure, many evaluations have to be performed.

After the solution of the forward problem, the measurements are synthesized in the output as a vector of $N_i = 25$ voltages measured along the bottom of the plate. This is noted as:

$$\text{Direct problem output} \rightarrow \phi_i^{FEM}; \quad i = 1, \ldots, N_i = 25 \tag{8}$$

4.3. Experimental measurement

The main goal of this work is to explore how the probabilistic nature of the system can be formulated and how it affects the damage search. The origin of the system indeterminateness lies in the uncertainties of the parameters in the governing equations of the material behaviour.

Tarantola (2005) distinguishes two kinds of probabilistic parameters, the *model parameters* and the *observable parameters*. The model parameters include the uncertainties condensed in the piezoelectric properties, i.e. the piezoelectric constitutive parameters, whereas the observable parameters randomness are expressed as uncertainties in measurements. Both magnitudes are therefore treated as random variables, instead of deterministic ones.

The uncertainties in the observations or measurements are formulated in two alternative ways: (I) adding a normally distributed noise level to the direct problem output (white noise), by means of generating random numbers with a normal probability and (II) developing a uncertainty analysis, namely, considering the material properties as random variables and using the FEM model to compute the ensuing random measurements. These two procedures can be formulated as:

(I) *Deterministic with random noise*

$$\text{Experimental measurement} \rightarrow \phi_i^{EXP_{(9)}} = \phi_i^{FEM} + \gamma_i RMS(\phi_i^{FEM})\psi \tag{9}$$

where γ_i are random variables generated by a *Gaussian* distribution of mean 0 and standard deviation 1, ψ is a parameter defined to control the noise level and *RMS* is the root mean square given by:

$$RMS(\phi_i^{FEM}) = \sqrt{\frac{1}{N_i}\sum_{i=1}^{N_i}\left(\phi_i^{FEM}\right)^2} \tag{10}$$

(II) *Probabilistic model-based*

$$\text{Experimental measurement} \rightarrow \phi_i^{EXP_{(11)}} = N(\mu_{\phi_i^{FEM}}, \sigma_{\phi_i^{FEM}}); \quad i = 1, \ldots, N_i \tag{11}$$

where N denotes an arbitrary distribution function and $\mu_{\phi_i^{FEM}}$ and $\sigma_{\phi_i^{FEM}}$ can be determined *a posteriori* by means of MCA, see Eq. (2).

The first procedure (also performed in Rus et al. (2006, 2008), Liu and Chen (1996), Lahmer et al. (2008) and Kaipio (2008)) has two limitations: (i) it assumes that the noise is normally distributed and (ii) the noise level ψ is an unknown magnitude. The second procedure has the inconvenient of requiring a large number of experiments, but, if the random variable distributions are accurate, it is a good technique to design the experiment (see Saltelli et al., 2000). To avoid these limitations, a goal of this work is to validate the first procedure as an acceptable approximation of the second one.

4.4. Cost functional

The cost functional (CF) is defined as the quadratic-difference between the experimental and FEM-predicted measurements:

$$f = \frac{1}{2N_i}\sum_{i=1}^{N_i}\left(\phi_i^{EXP} - \phi_i^{FEM}\right)^2 \tag{12}$$

where $N_i = 25$ is the number of measurement points and ϕ_i^{EXP} is $\phi_i^{EXP_{(9)}}$ or $\phi_i^{EXP_{(11)}}$, depending of the simulation method selected.

In contrast to gradient-based algorithms, for which the CF is defined as f, when the minimization is carried out by genetic or other heuristic algorithms, the CF is usually defined in an alternative way as f^L:

$$f^L = \log(f + \varepsilon) \tag{13}$$

where ε is a small non-dimensional value (here adopted as $\varepsilon = 10^{-16}$) that ensures the existence of f^L when f tends to zero. In addition, as it was argued in Gallego and Rus (2004), this new definition of the CF usually increases the convergence speed of the minimization algorithms.

4.5. Minimization

In order to minimize the CF and calculate the IP output, the minimization problem is formulated to find p_i such that,

$$\min_{p_i} f^L(\mathbf{p}) \tag{14}$$

Standard genetic algorithm (GA) is employed in this work to minimize the Eq. (14) and to obtain the IP output, which is a set of parameters that identify the position and extension of the defect. Other optimization techniques, like gradient-based algorithm, can be applied. However, in Rus et al. (2009) it was concluded that GA guarantees convergence, whereas gradient-based algorithm strongly depends on the initial guess that needs to be provided.

The GA is a heuristic optimization technique based on the rules of natural selection and genetics: *the superiors survive while the inferiors are eliminated*. A population of individuals (called chromosomes) is randomly generated. The population comprises a group of chromosomes which represent possible solutions in the problem space. Each individual is assigned a fitness or cost functional by computing the response corresponding to those parameters, for which one direct problem is solved independently, and comparing with the reference response. Genetic operators such as crossover and mutation are applied to obtain the child population. Finally, the child chromosomes with higher fitness replace some of their parent chromosomes. The process runs until a stopping criterion (like the number of generations) is reached.

The parameters used for the GA minimization are shown in Table 1. The selected population size should guarantee to find a global optimum at an adequate computational cost and genetic diversity has to be injected to the mutation and crossover parameters in order to ensure that the solution does not fall in local minima.

4.6. Probabilistic damage solution

The minimization algorithm in the previous section provides a deterministic output of the inverse problem as a fixed value of the damage characterization parameters. However, a probabilistic study of the IP solution is carried out by combining the latter with the MCA described in Section 5.2, where the model M (see Eq. (1)) is the IP algorithm (see Fig. 4).

Table 1
Parameters used for the GA minimization.

Parameter	Value
Population size	30
Crossover ratio	0.8
Mutation ratio	0.02
Number of generations	200

5. Results

5.1. Variables and notation

The voltage measured along the bottom of the plate (see Fig. 3) depends on: (i) the load (T_{xx}^{ap}), (ii) the specimen geometry (L_x, L_z, x_0, z_0 and r) and (iii) the material properties (see Eq. (6)). However, in this work, only the material properties are treated as random variables ξ_j.

Material properties are assumed to be normally distributed and uncorrelated with each other. This assumption also was performed by Ramamurty et al. (1986). The means are given by the *catalogue* properties of PZT-4 (see EFUNDA – Engineering Fundamentals, 2006), while the standard deviations (uncertainties) are assumed to be about 0.1% of the mean value.

Table 2 shows the problem variables with their random or deterministic character, the mean, the standard deviation (STD) and the standardized regression coefficients (SRC) notation.

5.2. Validation of Monte Carlo analysis

In order to validate the MCA, it is considered the simple problem consisting of the piezoelectric plate, described in Section 3, but without defect. For this problem, the voltage along the bottom of the plate is given by Palma (2006):

$$\phi^{ANA} = -g_{31}\left(1 - \frac{s_{12}^D}{s_{11}^D}\right) L_z T_{xx}^{ap} \tag{15}$$

The error propagation (EP) theory (see Bevington, 1969) allows to quantify the sources and magnitudes of errors involved in the measurements of voltages for the case without defect, where an analytical solution is available. Two types of errors can be studied: systematic and random errors. However, we only consider the second type, which can be dealt with in a statistical manner using the following relationship:

$$\sigma_{\phi^{ANA}} = \sqrt{\sum_{j=1}^{N_\xi} \left(\frac{\partial \phi^{ANA}}{\partial \xi_j}\right)^2 \left(\sigma_{\xi_j}\right)^2} \tag{16}$$

where $\sigma_{\phi^{ANA}}$ and σ_{ξ_j} are the standard deviations of the Eq. (15) and of the random variables, respectively.

Fig. 6 shows (a) the mean and (b) the standard deviation versus the sample size m when random sample (RS) and Latin hypercube sample (LH) are considered. The analytical solution obtained using the EP theory is superimposed on the figure to observe the convergence. On the one hand, Fig. 6a shows that the mean converges to the real value (represented by EP) faster using LH than RS. This results agree with the results obtained by McKay et al. (1979), who concluded that LH results are more stable estimates of the mean and standard deviation than random

Table 2
Deterministic and random variables for the problem. STD and SRC denote the standard deviation and the standardized regression coefficient, respectively.

Variable	Character	Mean	STD	Units	SRC notation
T_{xx}^{ap}	Deterministic	1	–	$\times 10^{3}$ [Pa]	–
L_x	Deterministic	6	–	$\times 10^{-2}$ [m]	–
L_z	Deterministic	6	–		–
s_{11}^D	Random	10.990	0.011	$\times 10^{-12}$ [m^2/N]	$\Theta_1 = \Theta_{s_{11}^D}$
s_{12}^D	Random	−5.360	0.005		$\Theta_2 = \Theta_{s_{12}^D}$
s_{13}^D	Random	−2.220	0.002		$\Theta_3 = \Theta_{s_{13}^D}$
s_{33}^D	Random	8.240	0.008		$\Theta_4 = \Theta_{s_{33}^D}$
s_{44}^D	Random	20.160	0.020		$\Theta_5 = \Theta_{s_{44}^D}$
g_{31}	Random	−10.690	0.011	$\times 10^{-3}$ [Vm/N]	$\Theta_6 = \Theta_{g_{31}}$
g_{33}	Random	25.110	0.025		$\Theta_7 = \Theta_{g_{33}}$
g_{15}	Random	37.980	0.040		$\Theta_8 = \Theta_{g_{15}}$
β_{11}^T	Random	7.660	0.008	$\times 10^{7}$ [Nm^2/C^2]	$\Theta_9 = \Theta_{\beta_{11}^T}$
β_{33}^T	Random	8.690	0.009		$\Theta_{10} = \Theta_{\beta_{33}^T}$

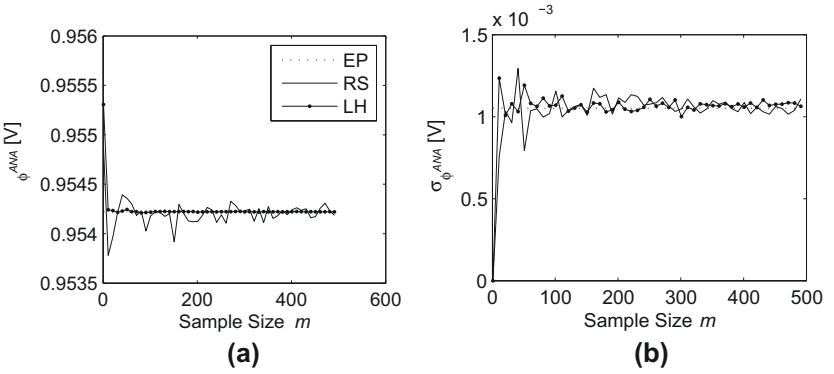

Fig. 6. (a) Mean and (b) standard deviation versus sample size for random sample (RS) and Latin hypercube sample (LH). EP shows the mean and standard deviation computed using the error propagation theory.

sampling. On the other hand, in Fig. 6b both sample types converge slowly. This test justifies the choice of LH for the MCA sampling.

A LH sample of 150 executions is considered the optimum sample size for this problem. Furthermore, for uncertainty and sensitivity analysis the LH sample is a good election as it was shown in McKay et al. (1979).

Table 3 shows the mean, standard deviation and standardized regression coefficients calculated using EP theory and the MCA with random sample m = 150 and solving the model M (now the plate without defect) by the FEM. All the results agree very well (low relative errors), validating our MCA implementation.

Table 3
Mean, standard deviation and standardized regression coefficients calculated using Monte Carlo analysis (model evaluated with the FEM code) and propagation error theory (analytical expression).

	MCA	EP	Relative error (%)
μ_ϕ [V]	0.9542	0.9542	0
σ_ϕ [V]	0.0011	0.0011	0
$\Theta_{s_{11}^D}$	−0.293	−0.292	0.34
$\Theta_{s_{12}^D}$	−0.273	−0.272	0.37
$\Theta_{g_{31}}$	−0.916	−0.917	0.11

5.3. Uncertainty of measurements

In order to develop an UA and a SA for the experimental voltage simulated, the MCA is applied for a piezoelectric plate with a defect inside. The defect is characterized by the coordinates $\tilde{x}_0 = 3.5, \tilde{z}_0 = 2$ and $\tilde{r} = 0.5$ [cm], while the material properties (mean and standard deviation) are given in Table 2. The model M is the particular plate (described in Section 3) with defect and its response is computed by the FEM. The sample size is m = 150.

Fig. 7a shows the voltage measured along the bottom of the plate versus the coordinate x for each measurement point. Three curves of the voltage are represented, using: the direct problem solution ϕ_i^{FEM}, the technique shows in Eq. (9) $\phi_i^{EXP_{(9)}}$ with ψ = 0.1% and the other one expressed in Eq. (11) $\phi_i^{EXP_{(11)}}$. Two deductions can be drawn: (i) the mean obtained with the MCA (represented by circles) agrees with the direct problem solution and (ii) the voltage simulated by $\phi_i^{EXP_{(9)}}$ falls between the error bars (standard deviation calculated using the MCA). On the other hand, Fig. 7b shows the *p-value*, obtained using the *Jarque–Bera* normality test (see Jarque and Bera, 1987), versus the measurement points. Since the probability is larger than the significance level (5%), the null hypothesis (*the data are normally distributed*) cannot be rejected. Therefore, a

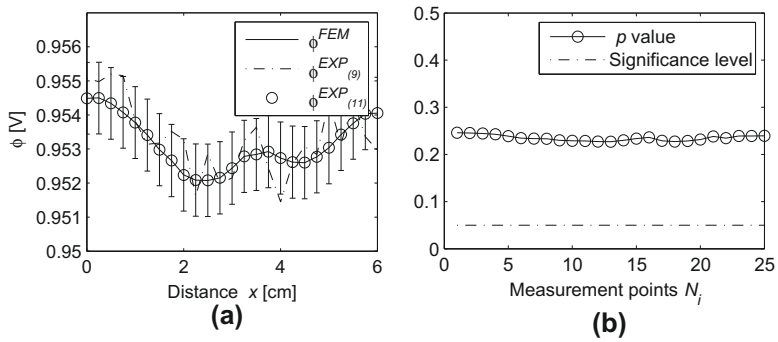

Fig. 7. (a) Voltage measured versus the coordinate x for each measurement point using the direct problem (solid line), the procedure shown in Eq. (9) (dotted line) and the other one shown in Eq. (11) (circle represents the mean and error bar the standard deviation). (b) *p-Value*, obtained using the *Jarque–Bera* normality test, versus the measurement points.

normal distribution $N(\mu_{\phi_i^{FEM}}, \sigma_{\phi_i^{FEM}})$ is obtained for each measurement point. This result is in accordance with the linearity of the model and the normal distribution of all the random variables. Furthermore, the standard deviations in each measurement point is about 0.1% of the mean value, which supports the value $\psi = 0.1\%$ used in Eq. (9) in order to obtain $\phi_i^{EXP_{(9)}}$. In conclusion, Eq. (9) used in Rus et al. (2009) is valid when $\psi = 0.1\%$. Therefore, the two hypothesis formulated in Section 4.3 and assumed in Rus et al. (2009), namely, normal distribution of the noise and that the noise level on measurements is of the same order of magnitude as the uncertainties in material constants, are now validated.

5.4. Sensitivity of measurements

Fig. 8 shows the standardized regression coefficients SRC (see notation in Table 2) in absolute value versus the measurement points, from which three observations can be made: (i) the measurements are most sensitive to the material properties s_{11}^D, s_{12}^D and g_{31}. These properties correspond to those that explicitly appear on the analytical solution without defect, see Eq. (15). This means that the total sensitivity is the sum of the sensitivity without defect and the alteration due to the defect. The large value of the first component is responsible for the overall magnitude of the sensitivity, which effectively masks the defect-dependent component. The largest sensitivity value corresponds to $|\Theta_{g_{31}}| \approx 0.9$, which agrees with the constitutive equations that directly relate g_{31} with the applied load T_{xx}^{ap} and the electric field E_z from which the electric voltage is measured (see Eq. (6)). Note that a purely piezoelectric effects is induced. (ii) The presence of the defect is responsible for a non-zero sensitivity to some material constants, that is null without defect (see Eq. (15)). These particular properties are: $g_{33}, g_{15}, \beta_{11}^T$ and β_{33}^T, and produce a sensitivity one order of magnitude smaller. Furthermore, the sensitivity is larger at the measuring points where the voltage alteration due to the defect is larger. This can be verified by looking at the first measuring point (coordinate 0). This measurement, whose value is close to that provided by the analytical expression, is least altered by the defect, and shows the smallest sensitivity, as predicted. On the other hand, the sensitivity is about three order of magnitude smaller for s_{13}^D. (iii) Finally, the measurements are not sensitive to two particular mechanical properties: s_{33}^D and s_{44}^D (only noise is shown on the corresponding figures).

To sum up, Fig. 9 shows all the SRC's in absolute value superposed and in logarithmic scale versus the measurement point. The three observations are clearly identifiable in this figure, since the curves corresponding to each observation appear to be grouped and follow three differentiated trends.

5.5. Effect of noise amplitude

In this section, the output of the IP is obtained minimizing the quadratic-type CF by means of GA for a defect characterized by $\tilde{\mathbf{p}} = (3.5, 2, 0.5) \times 10^{-2}$ [m]. In order to represent the IP solution versus the noise level, a *Distance* between predicted and real parameters is defined in an Euclidean sense as (see Rus et al., 2009):

$$Distance = \frac{\sqrt{\sum_{i=1}^{N} (\tilde{p}_i - p_i)^2}}{\sum_{i=1}^{N} \tilde{p}_i} \tag{17}$$

where N is the number of parameters to identify.

Fig. 10 shows the *Distance* from the identified damage parameters to the real one, as defined in Eq. (17), versus an increasing noise level controlled by the parameter ψ, see Eq. (9). Ten different realizations of the search (GA minimizations) are performed for each noise level, and the mean (circle) and the standard deviation (error bar) of the resulting distances are obtained. The figure shows how the deviation of the IP output steadily increases with the simulated noise. A standard noise level $\psi = 0.1\%$ is used in most of the analysis of this work, as a consequence of the assumption of 0.1% of standard deviation in the material properties. If the uncertainty in the material properties is different, the dependency of the IP output is shown to be adequately smooth for different levels of uncertainty. On the other hand, for noise level bigger than 0.5% the IP solution becomes unstable, because the cost function is distorted (see Fig. 11). Remember that the cost functional has multiple local minima, of which the absolute one is expected to match the real parameters. When the noise is large, other local minima surpass the expected one, and the solution becomes unstable.

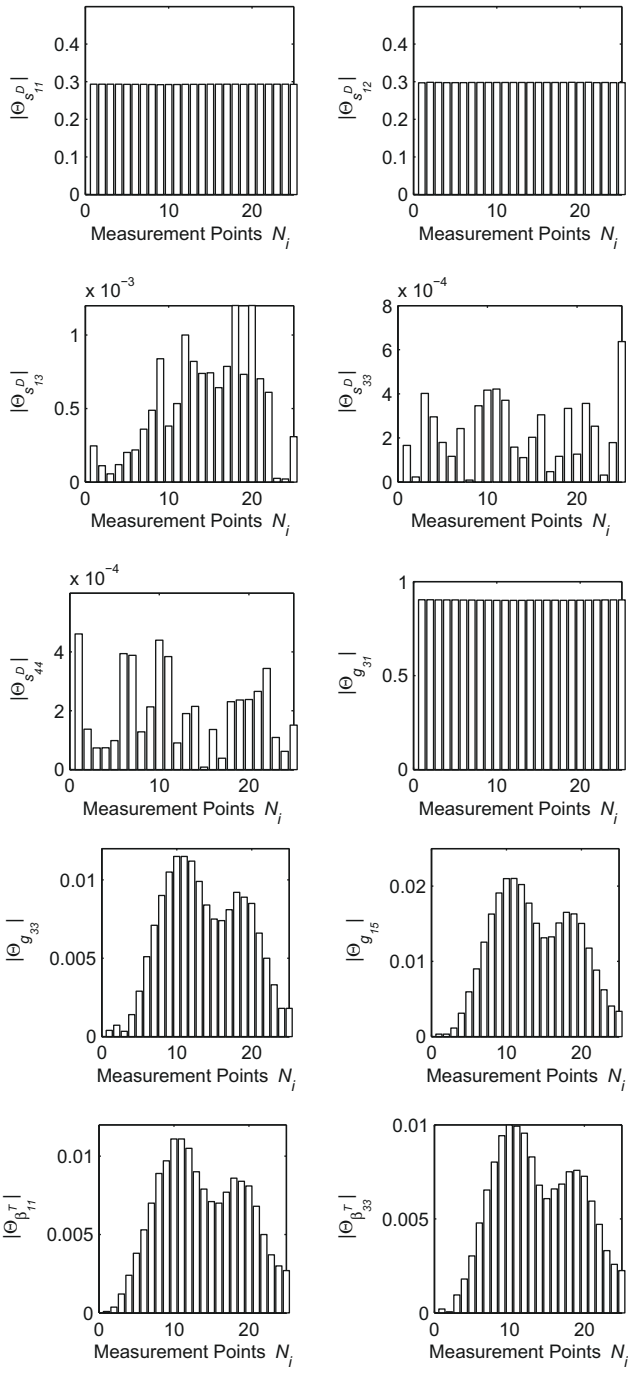

Fig. 8. SRC's in absolute value versus measurement points.

The error in the IP output is a combination of the errors originated by the uncertainty in the model (noise), the numerical errors of the model (FEM) and the error from the search algorithm (GA). For the case without noise, the error originated by the GA is about 5×10^{-5}, while the remaining error generated by FEM is about 4.8×10^{-4} (see Section 4.2). These figure conclude that the numerical tool errors are less significant than the error (noise) generated by the uncertainty in the model.

Fig. 11(left) shows the dependency of the cost functional on the spatial location of the defect (fixing the size at the real value) for increasing noise levels. If no noise is simulated, the cost function shows a clear optimum that the search algorithm is able to find. The shape of the cost function is distorted when the noise level increases in three significant ways: (i) the optimum becomes fuzzy and the area of admissible solutions larger, (ii) the shape of the fitness function becomes wavy (i.e. the gradient no longer points towards the

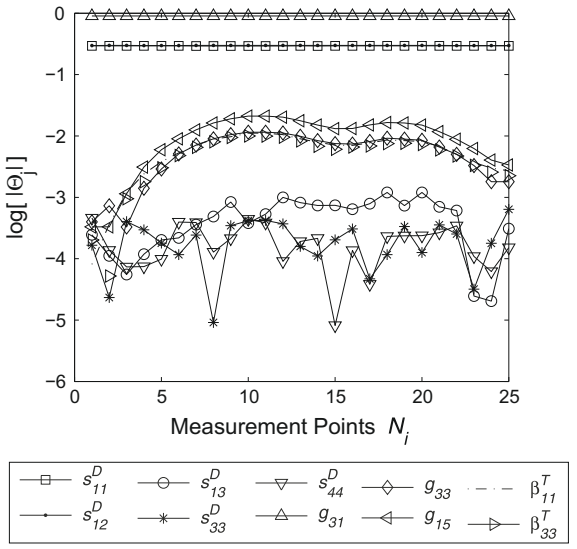

Fig. 9. SRC's in absolute value and in logarithmic scale versus measurement points. The most relevant sensitivities correspond to g_{31}, s^D_{11} and s^D_{12}.

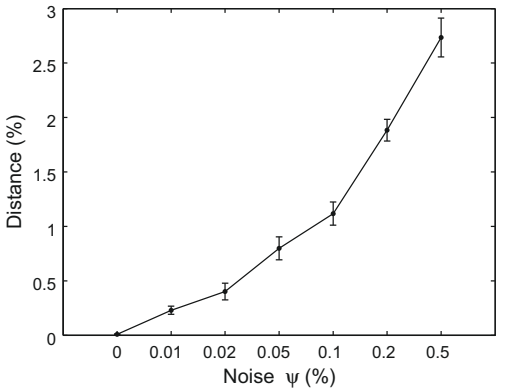

Fig. 10. *Distance* between computed and real results versus noise levels.

minimum), making the convergence process slower and more unstable and (iii) for large levels of noise, the optimum is located far from the real solution.

Fig. 11(right) shows the GA convergence for different noise levels. For the case $\psi \in (0, 0.1)\%$, the full convergence is obtained for less than 200 generations. A larger noise level is associated with slower convergence, probably due to the wavy and fuzzy shapes of the cost functional described above.

5.6. Study of the robustness of the method

The robustness and potentiality of the method has been studied evaluating a SA and obtaining an IP solution for a selection of different damage positions, 16, and for different damage areas, 10. Fig. 12 shows the different configurations studied to carry out the robustness analysis.

In order to show the SA results by scalar parameters, the calculated and measured voltages can be expressed by:

$$\phi_i^{FEM} \approx \theta_{i0} + \sum_{j=1}^{N_\xi} \theta_{ij}\xi_j$$
$$\phi_i^{EXP} = \phi_i^{FEM} \pm \sqrt{\sum_{j=1}^{N_\xi} \theta_{ij}^2 \sigma^2_{\xi_j}} \tag{18}$$

where the multiple linear regression approximation and the PE theory have been used. Replacing (18) into (12) and using the SRC definition (4):

$$f = \frac{1}{2N_i} \sum_{j=1}^{N_\xi} \lambda_j \tag{19}$$

where λ_j are the scalar parameters, which depends of the SRC of the random variable j and of the standard deviation of the measurement point i:

$$\lambda_j = \sum_{i=1}^{N_i} \Theta_{ij}^2 \sigma^2_{\phi_i} \tag{20}$$

Fig. 13 shows the λ_j parameters and the *Distance*, defined by (17), versus the damage position 1, 2, ..., 16 shown in Fig. 12. In order to obtain the λ_j, a SA is evaluated for each damage position. On the other hand, to obtain the *Distance* an IP is solved using GA and a noise level of $\psi = 0.1\%$ for each damage position. Fig. 14 shows the λ_j parameters and the *Distance* versus the damage area, see Figs. 12 and 9 for legend. The noise level used is $\psi = 0.1\%$.

From the two latter figures, the following conclusions can be extracted: (i) again, the largest sensitivities are those corresponding with the plate without defect, s^D_{11}, s^D_{12} and g_{31}. (ii) New components of sensitivity appear with the defect: $g_{15}, g_{33}, \beta^T_{11}$ and β^T_{33}, and their magnitude is correlated with the area of the defect; the remaining sensitivities are just due to noise. The sensitivities associated to the presence of a defect show little dependency on the position of the defect, and are significantly larger than those associated with noise, which means that at all positions, the defect can be successfully identified, as the *Distance* figure (on the right) shows. The *Distance* for all positions is around 1.1%, which is mainly due to the simulated noise $\psi = 0.1\%$ (see Fig. 10). It is also worthwhile to note that all *Distance* plots follow similar trends, and that the positions close to the boundary are easier to detect, which may be related to the application of the boundary conditions. (iii) The sensitivities associated to $g_{15}, g_{33}, \beta^T_{11}$ and β^T_{33} are actually those that allow to detect and locate the defect, and this can be verified by the fact that in the range of relative defect area 0.02–0.08, their magnitude coincides with that of noise, and for this range, the found *Distance* is also significantly larger (the IP does not converge successfully), whereas for larger areas, the *Distance* converges towards approximately 1% (when $\psi = 0.1\%$).

To sum up, this technique has been shown in theory to be able to detect the location and size of a damage for realistic errors, as shown in Fig. 13. The size or area is more difficult to identify than the location, and the smallest defect that can be found in theory is of the order of 0.08% with acceptable error, as shown in Fig. 14. These conclusions are corroborated by another perspective, the histograms in next section.

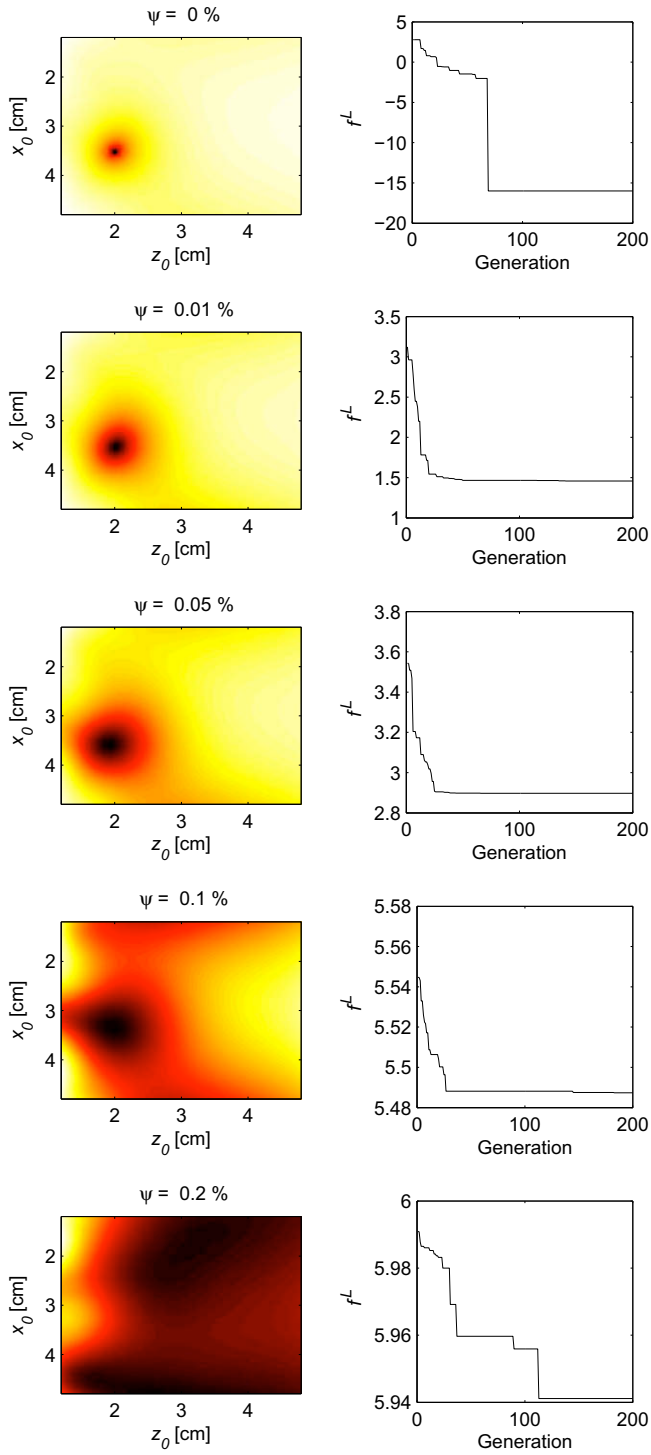

Fig. 11. Cost function and genetic algorithm convergence for different noise levels.

5.7. Effect of system uncertainty model in the IP output

There are two ways to increase the accuracy of the IP solution. The first one consists in decreasing the noise level, and this has been studied in Section 5.3. The second way consists on determining which material properties deteriorate the IP solution given a fixed experimental measurement, and this is the goal of the this section.

To analyze the effect of model uncertainties, the MCA is combined with the IP algorithm (the model M, see Eq. (1),

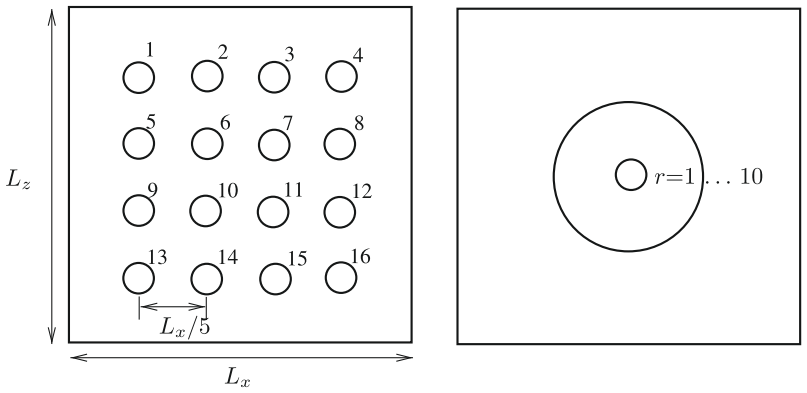

Fig. 12. Different damage positions and damage areas to carry out a robustness analysis.

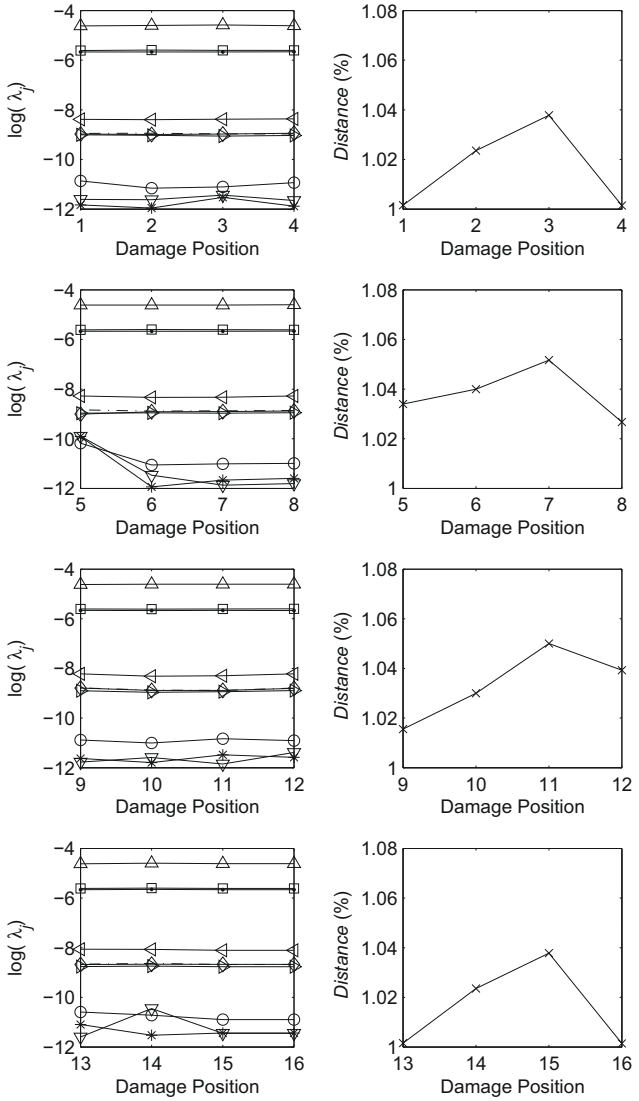

Fig. 13. λ_j and *Distance* versus damage position. For legend see Fig. 9.

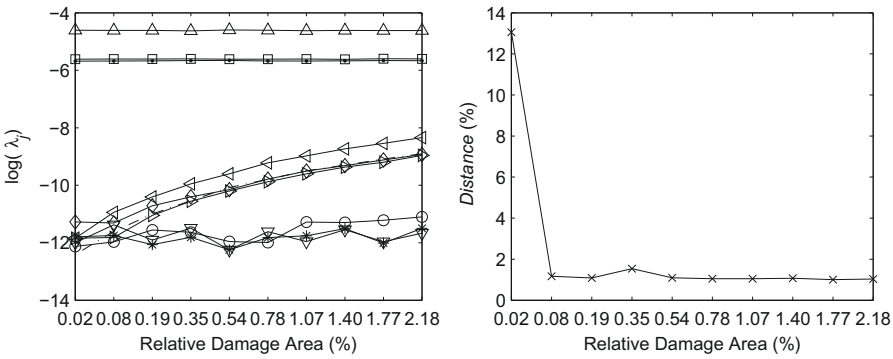

Fig. 14. λ_j and *Distance* versus damage area. For legend see Fig. 9.

is now the IP algorithm), considering the material properties as normally distributed values (see Table 2). In contrast with the deterministic IP algorithm, which considers deterministic model parameters to obtain the synthetic trial observations ϕ_i^{FEM} in Eq. (12), the probabilistic IP algorithm considers both terms ϕ_i^{EXP} and ϕ_i^{FEM} (experimental and trial observations) as probabilistic magnitudes. Therefore, the cost function f in Eq. (12) can be considered as a probabilistic function. Note that the goal of this formulation is to estimate which properties decrease the accuracy of the IP solution, while the aim of the Section 5.3 was to estimate which properties decrease the noise level. Hence, the MCA output, namely the probabilistic IP output, consist of scalar values, histograms, cumulative distributions functions and standardized regression coefficients for each of the three IP output parameters: x_0, z_0 and r.

In order to decrease the CPU time required to evaluate a sample size of the $m = 100$ by MCA, the minimization is now carried out by replacing the GA by the *BFGS* gradient-based algorithm (see Dennis and Schnabel, 1983). *BFGS* provides quicker convergence given a controlled initial guess. The drawback of *BFGS* compared to GA is that it is sensitive to the choice of random initial guess, and may not converge. In this problem, the initial guess is not taken as a random number, but replaced by the value $x_0 = 3.5$, $z_0 = 2$ and $r = 0.5$, which corresponds to the definition of the real problem: $\tilde{x}_0 = 3.5, \tilde{z}_0 = 2$ and $\tilde{r} = 0.5$ [cm], and should not be far from the IP solution when uncertainties are included. Note that this section is not interested in testing the robustness or convergence of the IP search, but to study the influence of the random character of the model parameters on the final IP solution.

Table 4 shows the scalar parameters obtained by means of the MCA (see Eq. (2)) and the *Distance* defined in Eq. (17) for the three IP output parameters and when the experimental measurement considered are the two procedures developed in this work. The *Distance* value is lower for $\phi_i^{EXP_{(11)}}$ than for $\phi_i^{EXP_{(9)}}$. Since the second consideration, $\phi_i^{EXP_{(11)}}$, is more realistic from an experimental point of view, the simple noise application used in Rus et al. (2009) ($\phi_i^{EXP_{(9)}}$) can be applied for theoretical or numerical studies, ensuring better results for future experimental studies.

Figs. 15 and 16 show the histograms and the cumulative distribution functions for the three parameters and for both experimental measurement considerations. According to this figure and for both considerations, the best scattering is attained for the parameter r and, therefore, this parameter is the more difficult to detect. On the other hand, the parameter x_0 is relatively easy of detect.

However, the most relevant conclusion is that the IP output using the probabilistic model formulation (Fig. 16) has a narrower dispersion and a clearer expected value (steeper cumulative distribution function and fewer outliers in the histogram) than when using the approximated model (Fig. 15). This proves that the approximated model defined in Eq. (9) comprises the final solution given by the fully probabilistic model, and provides a valid solution on the safe side. This observation extends the conclusion in Section 5.3, and validates the simplified semi-explicit formulation not only to estimate the uncertainties of the observations, but also of the final IP solution.

5.8. Sensitivity to system uncertainties in the IP output

Fig. 17 shows the standardized regression coefficients, in absolute value, for both types of experimental measurement simulations (see Table 2 for notation). The profiles of sensitivities are approximately the same for the three IP output and for the experimental measurement considerations, which further supports the conclusion in the previous section. Furthermore, these profiles also agree with the others obtained for the experimental measurements (see

Table 4
Scalar MCA parameters for the three IP output parameter and for both experimental measurement simulations.

Measurement type	x_0 [cm]		z_0 [cm]		r [cm]		*Distance*
	μ	σ	μ	σ	μ	σ	
$\phi_i^{EXP_{(9)}}$	3.55	0.03	2.11	0.09	0.45	0.15	0.018
$\phi_i^{EXP_{(11)}}$	3.52	0.06	2.04	0.08	0.54	0.14	0.016

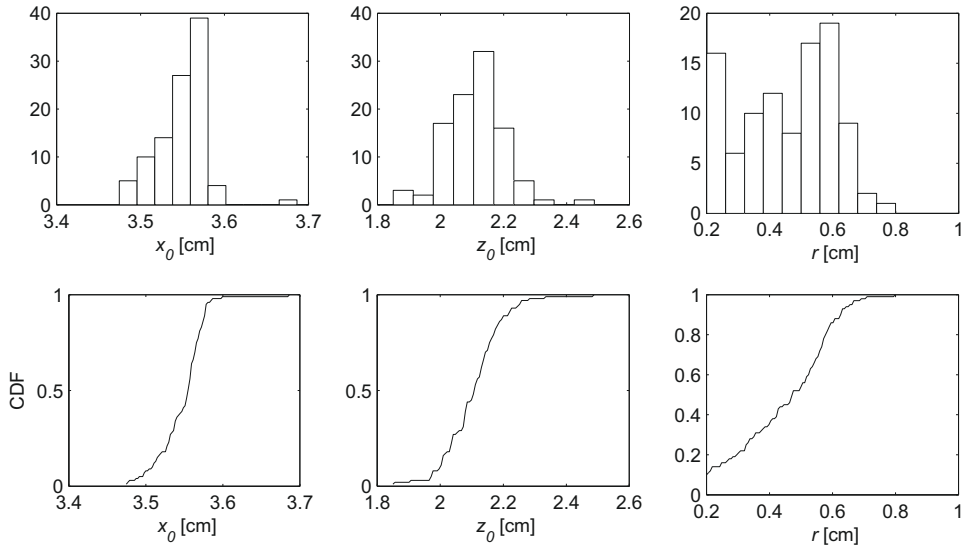

Fig. 15. Histogram and cumulative distribution function for the three IP output, considering $\phi_i^{EXP_{(9)}}$.

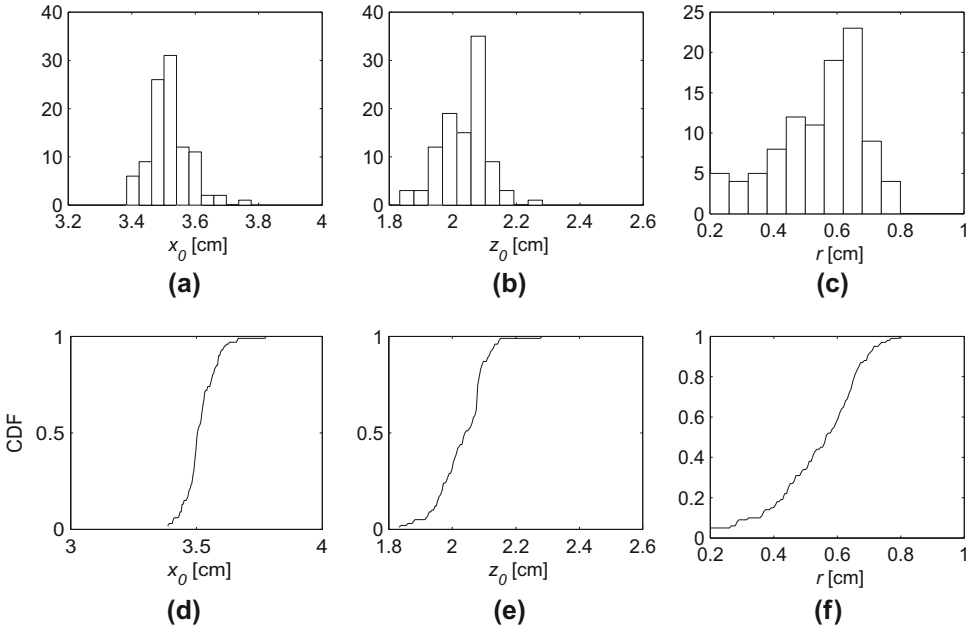

Fig. 16. Histogram and cumulative distribution function for the three IP output, considering $\phi_i^{EXP_{(11)}}$.

Section 5.3 and Figs. 8 and 9). Therefore, the parameters that increase the noise level and decrease the accuracy of the IP solution can be concluded to be the same that affect the measurements, namely, s_{11}^D, s_{12}^D and g_{31}.

6. Conclusion

A procedure to obtain the sensitivity of the measurements to material constant uncertainties in a model-based NDE system for piezoelectric ceramics has been developed and validated using Monte Carlo techniques, error propagation theory and with the help of an analytical solution. On the other hand, the Monte Carlo technique has been combined with the inverse problem algorithm in order to develop a probabilistic IP approach, where the probability distribution functions of the IP output have been obtained. A few conclusions are extracted.

For the experimental measurement study, the assumption that the noise on measurements is normally distributed is demonstrated as long as the uncertainty in material constants is normally distributed. Furthermore,

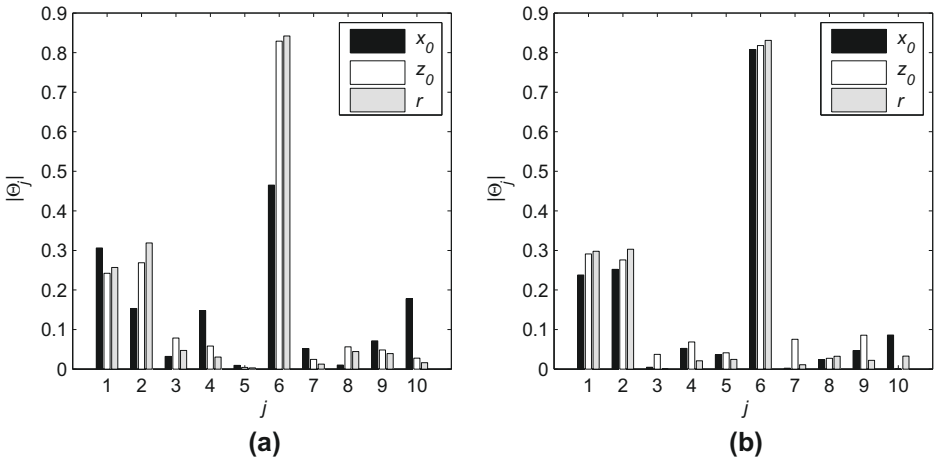

Fig. 17. Standardized regression coefficients in absolute value (see Table 2 for notation). Experimental measurement simulated by (a) $\phi_i^{EXP_{(9)}}$ and (b) $\phi_i^{EXP_{(11)}}$.

the magnitude of measurement noise is of the same order of magnitude as the material constants uncertainty.

For the probabilistic study, the detection of the coordinates of the center of the defect has been concluded as more easy to find. However, the radius of the defect is more difficult to find and a uncertainty treatment or a sophisticated minimization algorithm must be applied in order to obtain accurate results.

For both studies and as a practical conclusion, the uncertainty on the constants s_{11}^D, s_{12}^D and g_{31} should be controlled and reduced to accurately detect defects, since they are the most responsible ones of lack of sensitivity to the effect of the defect. In contrast, the measurements have been shown to be almost insensitive to uncertainties in constants s_{13}^D, s_{33}^D and s_{44}^D.

When assessing the robustness of this technique, the size or area is found to be more difficult to identify than the location, and the smallest defect that can be found within an acceptable error is of the order of 0.08% of area. Interestingly, the sensitivities associated to $g_{15}, g_{33}, \beta_{11}^T$ and β_{33}^T are found as those responsible of allowing the technique to detect and locate the defect, and their value determines such capability.

The inverse problem solution strongly depends of the noise level, which is evidenced by Fig. 10. Therefore, in order to increase the accuracy of the solution, the sensitivity analysis suggests that the uncertainty of the material constants s_{11}^D, s_{12}^D and g_{31} should be determined experimentally with a precision one or two orders of magnitude better than that of the rest of the properties.

The results obtained in this work are limited to the case of a simple damage type and to a 2-D model, in order to test new formulations while keeping low CPU times. Thus, extending these two limitations are the goal of our future work.

Acknowledgment

This research was supported by the Ministry of Education of Spain through Grant No. FPU AP-2006-02372.

References

Araújo, A.L., Mota Soares, C.M., Herskovits, J., Pedersen, P., 2002. Development of a finite element model for the identification of mechanical and piezoelectric properties through gradient optimization and experimental vibration data. Compos. Struct. 58 (5), 307–318.

Araújo, A.L., Mota Soares, C.M., Herskovits, J., Pedersen, P., 2006. Parameter estimation in active plate structures using gradient optimisation and neural networks. Inverse Prob. Sci. Eng. 14 (5), 483–493.

Bevington, P.R., 1969. Data Reduction and Error Analysis for the Physical Sciences. McGraw-Hill, New York.

Bonnet, M., Constantinescu, A., 2005. Inverse problems in elasticity. Inverse Prob. 21, R1–R50.

Charmpis, D., Scheller, G., 2006. Using Monte Carlo Simulation to Treat Physical Uncertainties in Structural Reliability: Coping with Uncertainty. Springer.

Clemen, R.T., Winkler, R.L., 1999. Combining probability distributions from expert in risk analysis. Risk Anal. 2, 187–203.

Cochran, W., 1977. Sampling Techniques. John Wiley & Sons.

Dennis, J.E., Schnabel, R.B., 1983. Numerical Methods for Unconstrained Optimization and Non-linear Equations. SIAM.

EFUNDA – Engineering Fundamentals, 2006. Materials Home. Efunda. Available from: <http://www.efunda.com/materials/piezo>.

Gallego, R., Rus, G., 2004. Identification of cracks and cavities using the topological sensitivity boundary integral equation. Comput. Mech. 33, 154–163.

Jarque, C.M., Bera, A.K., 1987. A test for normality of observations and regression residuals. Int. Stat. Rev. 16 (2), 1–10.

Kaipio, J., 2008. Modeling of uncertainties in statistical inverse problems. J. Phys. Conf. Ser.. doi:10.1088/1742-6596/135/1/012107.

Kaltenbacher, B., Lahmer, T., Mohr, M., Kaltenbacher, M., 2006. Pde based determination of piezoelectric material tensors. Eur. J. Appl. Math. 17 (4), 383–416.

Lahmer, T., Kaltenbacher, B., Schulz, V., 2008. Optimal measurement selection for piezoelectric material tensor identification. Inverse Prob. Sci. Eng. 16 (3), 369–387.

Liu, P.L., Chen, C.C., 1996. Parametric identification of truss structures by using transient response. J. Sound Vib. 191, 273–287.

Mayer, L.S., Younger, M.S., 1974. Procedures for estimating standardized regression coefficients from sample data. Sociol. Methods Res. 2 (4), 431–453.

McKay, M.D., Beckman, R.J., Conover, W.J., 1979. A comparison of three methods for selecting values of input variables in analysis of output from a computer code. Technometrics 21 (2), 239–245.

Montgomery, D.C., Runger, G.C., 1999. Applied Statistics and Probability for Engineers. John Wiley & Sons.

Oden, J.T., Belytschko, T., Babuska, I., Hughes, T.J.R., 2003. Research directions in computational mechanics. Comput. Methods Appl. Mech. Eng. 192, 913–922.

Ou, Z.C., Chen, Y.H., 2003. Discussion of the crack face electric boundary condition in piezoelectric fracture mechanics. Int. J. Fract. 123, L151–L155.

Palma, R., 2006. Estudio Numérico de Cerámicas Piezoeléctricas con Defectos. Grupo Mecánica de Sólidos y Estructuras. Universidad de Granada.

Pérez-Aparicio, J.L., Sosa, H., Palma, R., 2007. Numerical investigations of field-defect interactions in piezoelectric ceramics. Int. J. Solids Struct. 44, 4892–4908.

Ramamurty, U., Sridhar, S., Giannakopoulos, A.E., Suresh, S., 1986. An experimental study of spherical indentation on piezoelectric materials. Acta Mater. 47 (8), 2417–2430.

Ruíz, A., Ramos, A., San-Emeterio, J.L., 2004a. Estimation of some transducer parameters in a broadband piezoelectric transmitter by using an artificial intelligence technique. Ultrasonics 42, 459–463.

Ruíz, A., San-Emeterio, J.L., Ramos, A., 2004b. Evaluation of piezoelectric resonator parameters using an artificial intelligence technique. Integr. Ferroelectr. 63, 137–141.

Rus, G., Lee, S.Y., Chang, S.Y., Wooh, S.C., 2006. Optimized damage detection of steel plates from noisy impact test. Int. J. Numer. Methods Eng. 68 (7), 707–727.

Rus, G., Palma, R., Pérez-Aparicio, J.L., 2009. Optimal measurement setup for damage detection in piezoelectric plates. Int. J. Eng. Sci. 47, 554–572.

Saltelli, A., Chan, K., Scott, E.M., 2000. Sensitivity Analysis. John Wiley & Sons.

Sosa, H., Khutoryansky, N., 1996. New developments concerning piezoelectric materials with defects. Int. J. Solids Struct. 33 (23), 3399–3414.

Tarantola, A., 2005. Inverse Problem Theory. SIAM.

Tardieu, N., Constantinescu, A., 2000. On the determination of elastic coefficients from indentation experiments. Inverse Prob. 16, 577–588.

Taylor, R.L., 2005. FEAP A Finite Element Analysis Program: User Manual. University of California, Berkeley. Available from: <http://www.ce.berkeley.edu/~rlt>.